A Fictitious Domain Method for Numerical Homogenization

Tian Long He, Philippe Karamian, Daniel Choï

A Fictitious Domain Method for Numerical Homogenization

Tian Long He, Philippe Karamian, Daniel Choï[a]

[a] *Laboratoire de Mathématiques Nicolas Oresme ,*
Université de Caen
14032 Caen, France

Abstract

Numerical Homogenization gives numerical approximations of the effective properties of a composite material. In the case of periodic composite, multi-scale modeling allows to consider only a Representative Volume Element (RVE). In this paper, we propose an original finite element method based on fictitious domain principle, in which the RVE is represented by a structured mesh and the inclusions are represented by independent and non matching meshes. The integral computations on inclusions meshes are substituted into the structured mesh of the RVE, with the help of a connection matrix.

Keywords: Finite Element Method, Homogenization, Fictitious Domain Method

1. Introduction

A composite material is an heterogeneous material, composed of at least two different constituents : a matrix, usually serving as a binder, and inclusions made of one or more materials. The inclusions are often called reinforcements as the aim of manufacturing composite materials is to combine the properties of the matrix/inclusions to produce material with different properties from the individual constituents. To efficiently model such materials, numerical homogenization techniques allows the computation of the effectives properties.

We can distinguish two kinds of numerical homogenization techniques : mean field methods and full field methods [3, 19]. The mean field methods are analytic or semi-analytic methods, such as the Mori-Tanaka method or the self consistent method [8, 2]. They are used with an incomplete knowledge of the composite: only the volume fraction and the specific geometry of the inclusions are known. As they are based on the study of the Eschelby's tensor, see [4], they are usually restricted to spherical inclusions with low volume fraction. Full field methods consider more general composites, but require the exact knowledge of the geometry. Effective properties can be computed with multi-scale modelling [20], such as the finite element method [5] or iteratives methods based on Fast Fourier Transfom technique [16, 17]. These methods are valid for a periodic composite material. The material period is then identified as the Representative Volume Element (RVE).

As the RVE becomes more complex, especially in the cases with very thin or tiny inclusions or inclusions coated with a thin pellicle, some difficulties arise : to accurately model such RVEs, we need a huge number of meshes (especially in 3D) or a high resolution image. Although some numerical advances allow the study of very high resolution 3D images, the need to efficiently compute the effective properties of more and more complex RVE subsists.

In the case of finite element methods, one difficulty, due to the heterogenity, is to accurately approximate integrals defining the energy bilinear form involved in the weak formulation of the homogenization modeling see [20, 5, 14]. It usually requires a conforming mesh but the building such a conforming and periodic mesh with complex geometries is not trivial, see for instance [21].

To circumvent the meshing difficulty, several approaches have been considered, such as eXtended Finite Element Method [23, 15, 10] (XFEM), or Finite Cell Methods [11] (FCM). The XFEM is combined with the Level Set Method to define the inclusions and enriched shape functions [24]. The FCM considers only one structured mesh the elements of which are then called cells. The FCM uses cell subdivisions to ensure a better approximation of the integrals, see [11, 10].

Although considering periodic RVE based on multi-scale analysis rather than numerical homogenization with Kinetic or Stress Uniform Boundary Condition, the method presented in this paper has the same goal in the accurate approximation of integrals defining the energy bilinear form, but relies on computations with independent meshes based a Fictitious Domain principle: We use one structured mesh, for the entire RVE, including the matrix and the inclusions and non-structured independent meshes for the inclusions. We then compute integrals defined both on the whole RVE and integral defined on the inclusions. The inclusion meshes will be related to the structured mesh through a Connection Matrix. The Fictitious Domain Method for Homogenization (FDMH), proposed in this paper, can be directly applied to inclusions of any kind of shape or geometry, as long as a mesh is available.

The paper is organized as follows, after this short introduction we recall the periodic homogenization theory, based on a multiscale modeling and asymptotic developement. This periodic homogenization lead to variational problems that can be solved with the help of a classical finite element method. In section 3, we then introduce our new method based on fictitious domain principle to represent the inclusions. We describe the construction of a connection matrix which allows to connect the meshes and compute the energy forms involved in the periodic homogenization technique. In section 4, we show some numerical tests with different inclusion geometries, in order to evaluate and validate our method. We discuss the performance of our fictitious domain method for homogenization.

Notations

In this paper, scalar values are typed in italic whereas the vector values are typed in bold face.

Let us consider a εP periodic material. P constitutes the Representative Volume Element (RVE), ε denotes the characteristic length of the RVE. To fix the idea, we set the RVE $P = [0, 1]^3$. The multiscale modeling consider macrocospic and local space variables. To the macroscopic space variables $\mathbf{x} \in \mathbb{R}^3$, we associate the local (microscopic)

space variables:

$$\mathbf{y} = \frac{1}{\varepsilon}\mathbf{x} \in P.$$

The divergence and gradient differential operators are respectively denoted as

$$div = div_x + \frac{1}{\varepsilon} div_y,$$

$$\nabla = \nabla_x + \frac{1}{\varepsilon}\nabla_y,$$

where div_x and ∇_x (resp. div_y and ∇_y) denote the divergence and the gradient differential operator with respect to the macroscopic variables $\mathbf{x}$ (resp. the local variables $\mathbf{y}$).

2. Periodic Homogenization

In order to present our original method, we briefly recall here the periodic homogenization theory [14, 20] and its numerical implementation with the finite element method [5]. For the sake of simplicity, we present the theory and our method in the case of thermal properties. With a periodic heterogeneous media, the thermal constitutive law writes:

$$\mathbf{q} = \Lambda \nabla u, \tag{1}$$

where u denotes the temperature and $\mathbf{q}$ the heat flow, the conductivity tensor Λ is εP periodic.

Under the action of external heat source f, the thermal equilibrium writes:

$$div\ \mathbf{q} + f = 0. \tag{2}$$

We set the asymptotic expansion:

$$u = u^0(\mathbf{x}) + \varepsilon u^1(\mathbf{y}) + \dots \tag{3}$$

$$\nabla u = \mathbf{e}(u) = \mathbf{e}^0(u) + \varepsilon\, \mathbf{e}^1(u) + \dots \tag{4}$$

$$\mathbf{q} = \mathbf{q}^0 + \varepsilon \mathbf{q}^1 + \dots \tag{5}$$

As we develop:

$$\begin{aligned}\nabla u &= (\nabla_x + \frac{1}{\varepsilon}\nabla_y)(u^0 + \varepsilon u^1 + \varepsilon^2 u^2 + \dots) \\ &= \frac{1}{\varepsilon}\nabla_y u^0 + (\nabla_x u^0 + \nabla_y u^1) + \varepsilon(\nabla_x u^1 + \nabla_y u^2) + \dots,\end{aligned}$$

we obtain by identification:

$$\begin{aligned}\mathbf{e}^0(u) &= \nabla_x u^0 + \nabla_y u^1 \\ \mathbf{e}^1(u) &= \nabla_x u^1 + \nabla_y u^2 \\ \mathbf{q}^0 &= \Lambda(\nabla_x u^0 + \nabla_y u^1).\end{aligned}$$

Writing asymptotic expansion of the heat flow $\mathbf{q}$ in the equilibrium equation (2) gives, by identification, two distinct equations, a local equation and a macroscopic equation, see [20]. It follows that u^0 depends only on $\mathbf{x}$ and u^1 must be P-periodic. The local equation writes :

$$div_y(\mathbf{q}^0) = 0 \quad \text{in } P, \tag{6}$$

We write (6) in a weak or variational form :

$$\int_P \mathbf{q}^0 \nabla_y(u^*) = 0 \quad \forall u^* \in H^1_{per}(P) \tag{7}$$

Where $H^1_{per}(P)$ is the P-periodic Sobolev space H^1 .
Let $\mathbf{E}^0 = \nabla_x u^0$, then

$$\mathbf{q}^0 = \Lambda(\mathbf{E}^0 + \nabla_y u^1).$$

Averaging $\mathbf{q}^0$ on the RVE P, we then have :

$$\langle \mathbf{q}^0 \rangle = \int_P \Lambda(\mathbf{E}^0 + \nabla_y u^1) = \Lambda^h \nabla u^0. \tag{8}$$

Λ^h denotes the homogenized conductivity tensor.
Furthermore, with (7), $\forall \mathbf{E}^* \in \mathbb{R}^3$ and $\forall u^* \in H^1_{per}(P)$:

$$\begin{aligned} \int_P \mathbf{q}^0(\mathbf{E}^* + \nabla_y u^*) &= \int_P \mathbf{q}^0 \mathbf{E}^* + \int_P \mathbf{q}^0 \nabla_y u^* \\ &= \langle \mathbf{q}^0 \rangle \mathbf{E}^* \\ &= \Lambda^h \nabla u^0 . \mathbf{E}^* \end{aligned}$$

In other words, we obtain the variational problems:

$$\int_P \Lambda(\mathbf{E}^0 + \nabla_y u^1).(\mathbf{E}^* + \nabla_y u^*) = \Lambda^h \mathbf{E}^0 . \mathbf{E}^* \quad \forall u^* \in H^1_{per}(P), \forall \mathbf{E}^* \in \mathbb{R}^3. \tag{9}$$

The resolution of the three problems (9) as $\Lambda^h \mathbf{E}^0$ span $\mathbb{R}^3$, gives the homogenized conductivity tensor Λ^h. The variational problems (9) are well-posed [20] and their solutions can be approximated by the finite element method [5].

3. Fictitious Domain Method

The fictitious domain method is a technique used to solve elliptic boundary value problems in domain with complex boundaries or interfaces for which the meshing or the repetition of the meshing can induces difficulties[7]. To remedy this, distinct meshes are considered, one main mesh, usually structured, and meshes of the interfaces or inclusions. The fictitious domain method is then equivalent to a quadratic optimization problem with a linear constraint : the relations between the meshes or the interface or boundary conditions are taken in account with the help of Lagrange multipliers, see [7]. The method presented here differs since we shall not introduce Lagrange multipliers and we employ a true mesh of the inclusion instead of refining

the computation within the element (or cell) that are being cut by the boundary of an inclusion see [11, 10]. Actually, the use of isoparametric element on a structured mesh of the RVE allows us to connect the different meshes in a very simple way with the help of a Connection Matrix.

Energy form

We present our method in the case of thermal properties, the extension for other cases such as linear elasticity is straightforward.

From the variational problem (9) let us consider the quadratic energy functional:

$$J(u, \mathbf{E}) = \int_P \Lambda(\mathbf{E} + \nabla_y u).(\mathbf{E} + \nabla_y u). \tag{10}$$

To fix the idea, we suppose the RVE P to be constituted by two homogeneous and isotropic media : the matrix $P \setminus S$ and one inclusion S. The conductivity matrix writes:

$$\Lambda(y) = \begin{cases} \Lambda_m & in\ P\backslash S \\ \Lambda_s & in\ S. \end{cases}$$

We have :

$$J(u, \mathbf{E}) = \int_{P\setminus S} \Lambda_m(\mathbf{E} + \nabla_y u).(\mathbf{E} + \nabla_y u) + \int_S \Lambda_s(\mathbf{E} + \nabla_y u).(\mathbf{E} + \nabla_y u). \tag{11}$$

We then rewrite :

$$J(u, \mathbf{E}) = \underbrace{\int_P \Lambda_m(\mathbf{E} + \nabla_y u).(\mathbf{E} + \nabla_y u)}_{J_m} + \underbrace{\int_S (\Lambda_s - \Lambda_m)(\mathbf{E} + \nabla_y u).(\mathbf{E} + \nabla_y u)}_{J_s} \tag{12}$$

The main idea of the FDMH consists in defining two distinct and *a priori* incompatible and independent meshes representing the RVE P and the inclusion S. The consideration of these meshes allow independent numerical computations of J_m and J_s : Along the structured mesh of the entire domain P, let us define the interpolation space V^h of dimension n such that any $u^h \in V^h$ can be represented by $\hat{u} \in \mathbb{R}^n$. The functional J_m can then be defined with the help of a $(n + 3) \times (n + 3)$ matrix K_m :

$$J_m(u^h, \mathbf{E}) = \int_P \Lambda_m(\mathbf{E} + \nabla_y u^h).(\mathbf{E} + \nabla_y u^h) = \begin{bmatrix} \hat{u} \\ \mathbf{E} \end{bmatrix}^\top K_m \begin{bmatrix} \hat{u} \\ \mathbf{E} \end{bmatrix}. \tag{13}$$

On another hand, let us consider a conforming mesh of the inclusion S and let us define the interpolation space W^l. Let p be the dimension of W^l, any $v^l \in W^l$ can be represented by a vector $\hat{v} \in \mathbb{R}^p$. In order to simplify the presentation, the meshes will be denoted respectively as P and S.

The functional J_s can be defined in W^l with a $(p + 3) \times (p + 3)$ matrix K_s :

$$J_s(v^l, \mathbf{E}) = \int_S (\Lambda_s - \Lambda_m)(\mathbf{E} + \nabla_y v^l).(\mathbf{E} + \nabla_y v^l) = \begin{bmatrix} \hat{v} \\ \mathbf{E} \end{bmatrix}^\top K_s \begin{bmatrix} \hat{v} \\ \mathbf{E} \end{bmatrix}. \tag{14}$$

Both the matrices K_m and K_s can be computed using standard finite element procedures.

A Connection Matrix

As we defined the matrices K_m and K_s, the main difficulty is to connect the Degrees of Freedom (DOFs) $\hat{v}$ of the inclusion S to the DOFs $\hat{u}$ of the structured mesh P. With isoparametric elements, this can easily be achieved:
For each component v_i of $\hat{v}$, we have $v_i = v(N_i)$ where N_i is a node of S. Let E_l, be an element of the RVE P in which the node N_i is included, see Figure 1. Let $\hat{x}$, $\hat{y}$,

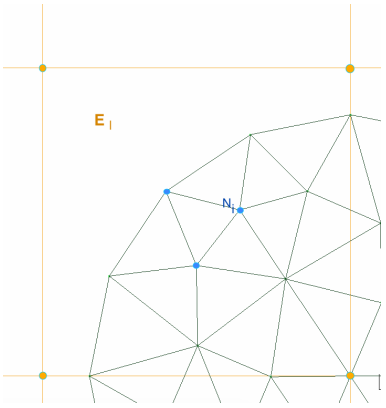

Figure 1: A node N_i from a triangular mesh of an inclusion in the quadrangular element E_l of the RVE

$\hat{z}$ be the coordinates of the nodes constituting the element E_l. With an isoparametric element, we usually define a reference element and its corresponding shape functions $\widehat{\Phi}$. Let (x, y, z) be the coordinates of the node N_i, and let (r, s, t) be its coordinates in the reference element associated to E_l. By definition, we have :

$$x = \widehat{\Phi}(r, s, t)^\top \hat{x}$$
$$y = \widehat{\Phi}(r, s, t)^\top \hat{y}$$
$$z = \widehat{\Phi}(r, s, t)^\top \hat{z}$$

Let v_i be the value of v^l at node N_i :

$$v_i = v(x, y, z) \tag{15}$$

As we work with isoparametric elements, we also have :

$$v(x, y, z) = \widehat{\Phi}(r, s, t)^\top \hat{u}, \tag{16}$$

In other words, we have the relation from the value v_i at a node of the inclusion mesh to the values $\hat{u}$ on the mesh of the element E_l :

$$v_i = \widehat{\Phi}(r, s, t)^\top \hat{u}. \tag{17}$$

We fill up (completing with zeroes) the relation (17) to all the values of u in the mesh of the RVE P and let us denote with C_i the $1 \times n$ line matrix such that :

$$v_i = v(x, y, z) = \widehat{\Phi}(r, s, t)^\top \hat{u} = C_i \hat{u},$$

($\hat{u}$ abusively represents the nodal values of u in an element E_l but also in the whole RVE P). Considering every nodes of S, we finally obtain a connection matrix C constructed line by line, which connects $\hat{v}$, the DOF associated to the mesh of the inclusions, to $\hat{u}$, the dof associated to the mesh of the RVE :

$$\hat{v} = C\hat{u}. \tag{18}$$

We are then able to rewrite the energy quadratic form computed on the inclusion J_s :

$$J_s = \begin{bmatrix} \hat{v} \\ \mathbf{E} \end{bmatrix}^\top K_s \begin{bmatrix} \hat{v} \\ \mathbf{E} \end{bmatrix} = \begin{bmatrix} C\hat{u} \\ \mathbf{E} \end{bmatrix}^\top K_s \begin{bmatrix} C\hat{u} \\ \mathbf{E} \end{bmatrix}. \tag{19}$$

Finally, we obtain the main energy quadratic form defined only on $\hat{u}$:

$$J(u, \mathbf{E}) = \begin{bmatrix} \hat{u} \\ \mathbf{E} \end{bmatrix}^\top \left(K_m + \begin{bmatrix} C & 0 \\ 0 & 1 \end{bmatrix}^\top K_s \begin{bmatrix} C & 0 \\ 0 & 1 \end{bmatrix} \right) \begin{bmatrix} \hat{u} \\ \mathbf{E} \end{bmatrix}. \tag{20}$$

In other words, with the matrix defined in (20), we are applying a finite element method to the problems of (9) with the interpolation space defined on the structured mesh of the RVE P.

In case of multiple inclusions, the procedure is repeated independently for each inclusion; all computations can be performed in parallel. The principle is very general and flexible, the inclusion meshes do not have to be of identical types, we can mix different types of mesh.

A priori, for unstructured meshes, the determination of the connection matrix C is not trivial. This difficulty is completely relieved, in the case of structured mesh for the RVE, with the use of isoparametric elements. In such cases, a simple formula (17) gives every components of the matrix C based on the definition of the shape functions of the reference element. Furthermore, with a regular structured mesh of P the periodic boundary condition are easily imposed by a simple substitution procedure.

It should be noted that since the material are heterogeneous, the discontinuity of the constitutive law implies that our FDMH solution, as it is not enriched, does not possess the correct weak continuity at the interfaces, except in the case where the distinct meshes are matching, see the test with a cubic inclusion in section 4.2. In the general case (non matching meshes) our method can be seen as conforming the discontinuity but for an approximated inclusion geometry. The approximation of the geometry is equivalent to a pixelization of the inclusion. Thus, the convergence of the method is ensured since a finer RVE mesh induces a better approximation of the inclusion.

4. Numerical tests

In order to validate the FDMH, we present here some numerical tests. We study thermal and linear elastic cases. For the sake of simplicity, we consider isotropic constitutive laws. We define a contrast parameter as the ratio between the characteristic coefficient of inclusions and that of RVE :

- In the thermal case

$$c_{thermal} = \frac{\lambda_{inc}}{\lambda_{rve}}$$

- In the linear elasticity case

$$c_{elastic} = \frac{E_{inc}}{E_{rve}}$$

where λ_{inc} and E_{inc} (resp. λ_{rve} and E_{rve}) are the conductivity and the Young's modulus of the inclusion (resp. the matrix). In all cases presented in this paper, we chose to set the contrasts $c_{thermal}$ and $c_{elastic}$ to 100.

We consider periodic RVE defined with inclusions of elementary geometry such as sphere, cube, and ellipsoid, To fix the ideas, we chose the 8-nodes hexaedric element (cub8) both for the inclusions and the RVE P, see Figure 2.

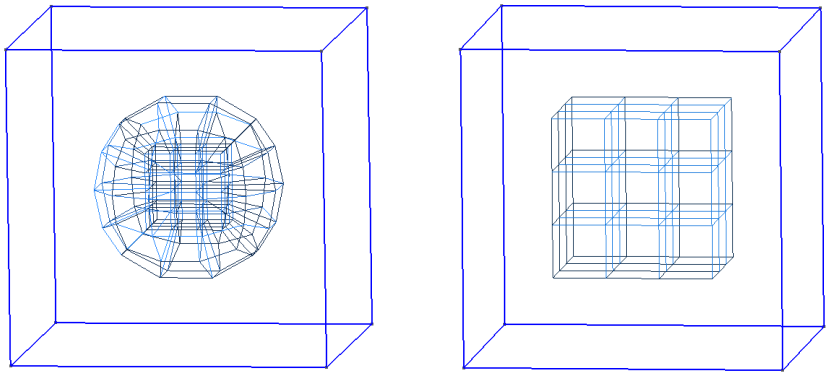

Figure 2: Spherical (left) and cubic (right) inclusions in hexaedric mesh

The structured mesh of the RVE is characterized by its resolution. A resolution n corresponds to a $n \times n \times n$ subdivision in all three space dimension. For instance, a resolution 10, represents a $10 \times 10 \times 10$, 8-nodes hexaedric mesh of the RVE, which contains 1000 elements, 1331 nodes, 1334 DOFs in the thermal case, and 3999 DOFs in the elasticity case. In the following, the RVE mesh resolution shall be denoted as N_{rve}. Associated to the resolution, we define the parameter $h_{rve} = 1/N_{rve}$, representing the characteristic length of an element of the mesh.

Besides the RVE resolution N_{rve}, we define another parameter N_{inc} to set the element size of the mesh of the inclusions. As h_{rve} and h_{inc} are respectively the characteristic length of the mesh of the RVE and the inclusion, we define the ratio η as :

$$\eta = \frac{h_{rve}}{h_{inc}}. \tag{21}$$

A value of η larger than 1 means a finer mesh of the inclusion than the RVE's. A serial of numerical tests have been performed to evaluate the influence of η on the results. We found out that, as we increase the value of η, the relative error is decreasing to 0. However, the evolution of relative error becomes negligible from the point $\eta = 1$, we illustrate this in Figure 3 in the case of spherical inclusion. On the other hand, a large value of η means a finer inclusion mesh and thus a longer time to complete the computations.

As the geometry can be complex, we also imposed a minimal resolution for the inclusions meshes. Hence for low RVE resolution, the parameter η can actually be greater than 1, in order to ensure a correct approximation of the geometry. Moreover, the meshing of the inclusion must be refined enough compared to the RVE meshing : a finer inclusion mesh avoids holes in the connections. This is a standard requirement in Fictitious Domain Methods. In other words, the mesh of the inclusion must be sufficiently refined compared to the resolution of the RVE, but need not to be too fine since that does not improve the approximation beyond a certain value. In all of our following numerical studies, the ratio η is set to the "optimal" value $\eta = 1$.

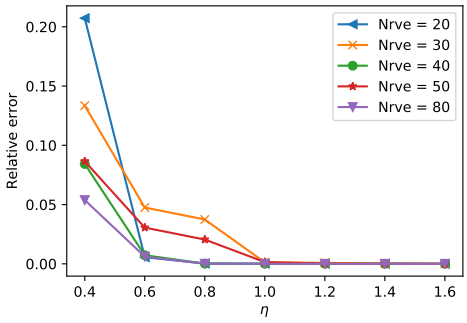

Figure 3: Relative error of the homogenized bulk modulus against the value of η for different RVE resolutions, in the case of a spherical inclusion

4.1. Spherical inclusion

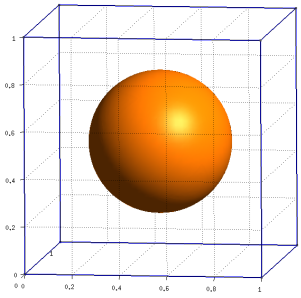

Figure 4: RVE with one spherical inclusion of diameter $d = 0.6$, volume fraction $\rho = 0.1131$

A sphere is defined by the coordinates of its center and its diameter d. In this example, we set $d = 0.6$, the volume fraction is thus $\rho = 0.1131$, see Figure 4. Since ρ is small enough, the analytical Mori-Tanaka model, based on the Eschelby's tensor is used as the reference solution [8], both in thermal and linear elasticity cases, see [22, 18].

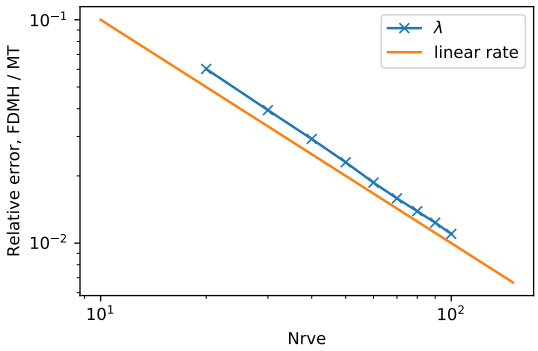

Figure 5: Relative error of computed homogenized conductivity coefficient λ for one spherical inclusion

In Figure 5, we draw the relative error of homogenized conductivity coefficient λ between the FDMH and the reference solution, the contrast $c_{thermal} = 100$. Linear convergence is observed with respect to the RVE resolution. With a resolution $N_{rve} = 100$ for the RVE, the relative error is about 1%.

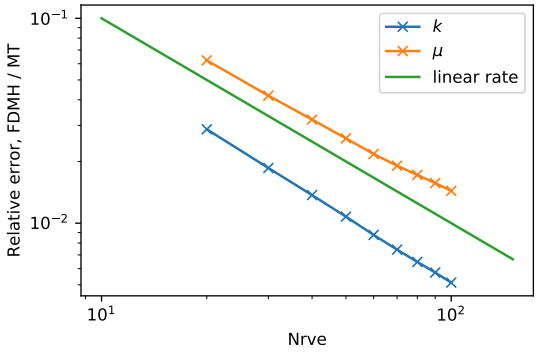

Figure 6: Relative error of computed homogenized elasticity coefficient k and μ for one spherical inclusion

In the linear elasticity case, the contrast $c_{elastic}$ is also set to 100. The Poisson's ratio is fixed as $\frac{1}{3}$ for both the inclusion and the matrix.

As the composite material is isotropic, we use the bulk modulus k and the shear modulus μ to represent the homogenized results. In Figure 6, the relative error of the homogenized elastic coefficient k and μ are plotted versus the RVE resolution. We notice a linear convergence with respect to the RVE resolution for both homogenized coefficients k and μ, which is similar to the thermal case.

We end this section with the case of one spherical inclusion of various size, the contrasts remain fixed at $c_{thermal} = c_{elastic} = 100$. We plot the comparative results

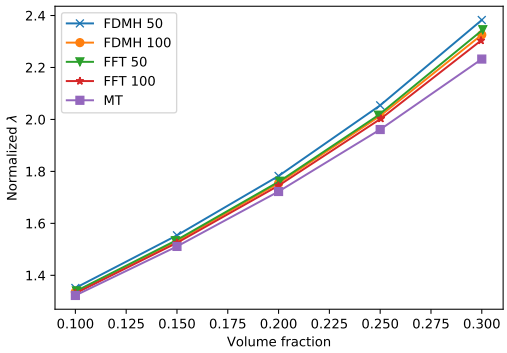

Figure 7: Comparison of normalized effective conductivity computed by Mori-Tanaka Model, FDMH, FFT at resolution 50 and 100 in the case of one spherical inclusion of different size

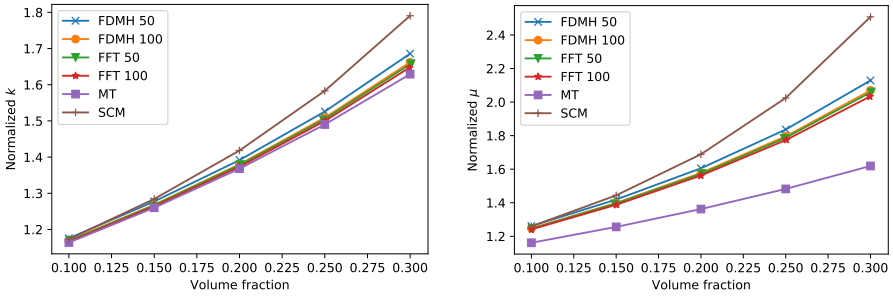

Figure 8: Comparison of normalized effective elastic properties computed by Mori-Tanaka analytic Model (MT), Self Consistent semi-analytic model (SCM), FDMH, FFT at resolution 50 and 100 in the case of one spherical inclusion of different size; bulk modulus (left) and shear modulus (right).

of the normalized conductivity (thermal case), see Fig. 7, and normalized bulk and shear modulii (elasticity case), see Fig. 8 between the Mori-Tanaka analytic model, the FDMH and the FFT method with different resolutions (50 and 100). We note that for greater volumic fraction the results given by the FDMH method deviate from analytical references (Mori-Tanaka and self-Consistent Model) but remain close to the results given by the FFT method.

4.2. Cubic inclusion

In this section, we consider a cubic inclusion. A cube of side $l = 0.5$ is placed at the center of RVE, as shown in Figure 9. The volume fraction of the inclusion is $\rho = 0.125$.

The iterative methods based on the FFT (Fast Fourier Transform) give in this case an almost exact solution since the geometry is exactly reproduced by the voxelisation, see [16]. For example, if we consider a centered cubic inclusion of side 0.5, the voxelizations should be made in multiple of 4 subdivisions in order to match the geometry.

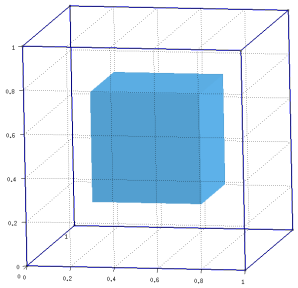

Figure 9: RVE with one cubic inclusion of side $l = 0.5$, volume fraction $\rho = 0.125$

In such cases, the FFT calculation (with a voxelization resolution 100) is then considered as a reference solution. We emphasize also that in such resolution, the FDMH will coincide exactly with a standard Finite Element Method (FEM) with conform and compatible mesh for the inclusion, see Figure 10, where the inclusion is represented in green and RVE in yellow.

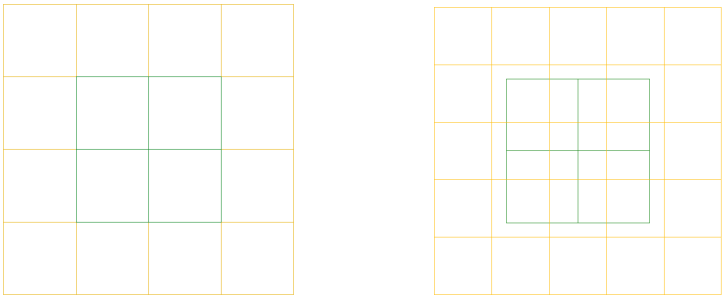

Figure 10: A cubic inclusion with matching (left, $N_{RVE} = 4$) and non-matching (right, $N_{RVE} = 5$) meshes.

In Figure 11, we have plotted the relative error of the homogenized thermal coefficient λ against the RVE resolution. In both matching and non-matching case, we notice a linear convergence. A noticeable difference in the order of magnitude for the relative errors can be observed in these two cases. This difference corresponds to the error made by the FDMH compared to a pure finite element calculation.

In Figure 12, the relative error of homogenized coefficient k and μ is plotted versus the RVE resolution. The same observation is found as in the thermal case, with a similar linear convergence.

Comparison between matching and non-matching meshes allows us to measure the error made by the FDMH compared to a conventional finite element method. We propose here a specific way to measure this error: in a fixed RVE mesh, from a matching position of two meshes, we move the cubic inclusion slightly in different directions (following x/y, in the xy plane or in the xyz space), until another matching position.

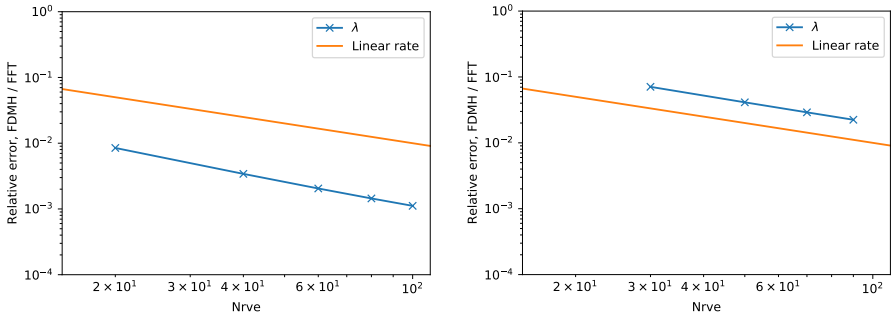

Figure 11: Relative error of the homogenized coefficients λ for one cubic inclusion, the mesh of inclusion and RVE are matching (left) or not matching (right)

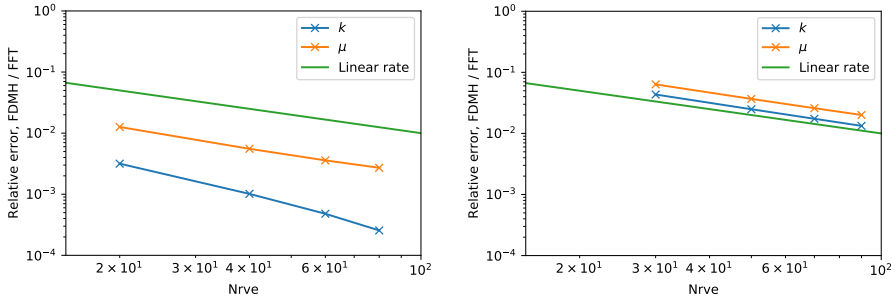

Figure 12: Relative error of the homogenized elastic coefficients k and μ for one cubic inclusion, the mesh of inclusion and RVE are matching (left) or not matching (right)

In Figure 13, we plot the FDMH / FEM comparison of the homogenized coefficients λ against the relative distance, which is the ratio between the moved distance and h_{rve}, the characteristic length of the mesh of the RVE. Compared to FEM, the error made by our method is null in the matching position, and reach its maximum with a relative distance equal to 0.5. For a resolution 100, the error of the method might be significant but is less than 2%.

4.3. Ellipsoidal inclusion

Let us consider an ellipsoidal inclusion. It is defined by its center coordinates and its principal axis or it can be defined as a volume the boundary of which can defined by a quadric :

$$\frac{x^2}{a} + \frac{y^2}{b} + \frac{z^2}{c} = 1.$$

We consider here an ellipsoid centered in the middle of the RVE P with $a = 0.15, b = 0.15, c = 0.4$, see in Figure 14. The volume fraction is $\rho = 0.0377$. Material constituted

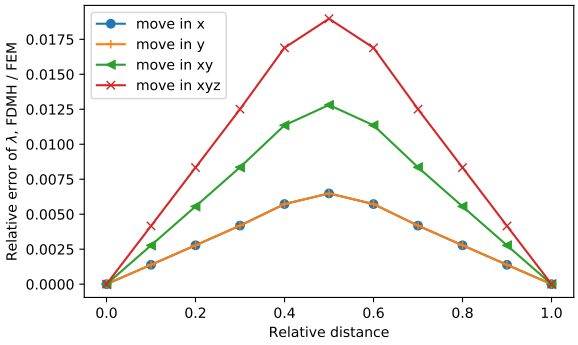

Figure 13: FDMH / FEM comparison between matching and non-matching meshes, for RVE with a cubic inclusion, thermal case

with such RVE are not isotropic, especially if the contrast is large. Thus, for the thermal case, we analyze the diagonal terms of the homogenized conductivity tensor Λ. For the elastic case, since we have a transversely isotropic material in the plane (**x**, **y**) and in the longitudinal axis (**z**), the computation of the compliance tensor S in the Bechterew base [1], makes it possible to identify Young's modulus E_1, E_3 and shear modulus G_{31}.

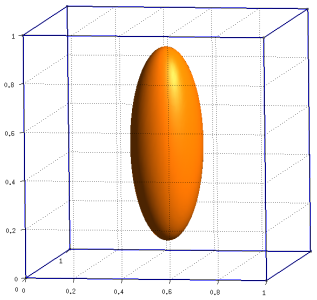

Figure 14: RVE with one ellipsoidal inclusion, $a = 0.15, b = 0.15, c = 0.4$, volume fraction $\rho = 0.0377$

Since a Mori-Tanaka solution is available [2], we use it as a reference solution. The linear convergence can be found in both cases for the coefficients in the plane (**x**, **y**), see Figure 15. The non-linear convergence of the coefficient in the longitudinal axis (**z**) is possibly caused by the inaccuracy of the referenced Mori-Tanaka solution, in the case of which, the inclusion is too elongated in the longitudinal direction compared to the size of RVE. With a RVE resolution of 100^3, the relative error is in order of magnitude 10^{-2}, see Figure 15.

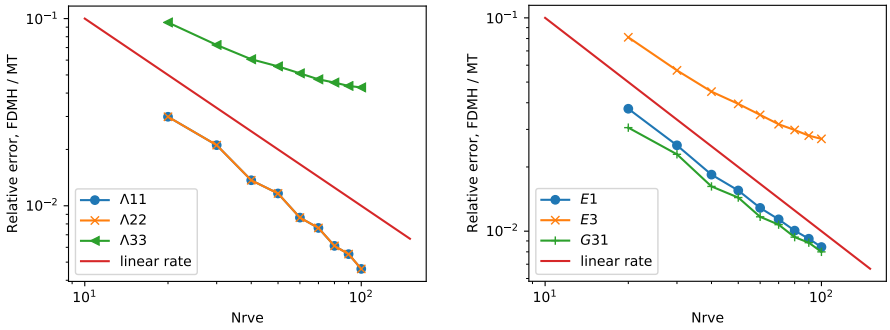

Figure 15: Relative error of the homogenized conductivity tensor (left) and stiffness coefficients (right) for one ellipsoidal inclusion case

4.4. Multiple ellipsoidal inclusions

To illustrate a case of mutiple inclusions, we consider another case of eight ellipsoidal inclusions with the same size $a = 0.05, b = 0.05, c = 0.15$, which are randomly distributed, see Figure 16. The volume fraction is $\rho = 0.01257$. We recall that the FDMH procedure, see section 3, is repeated for each inclusion.

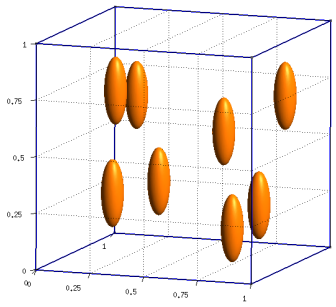

Figure 16: RVE with eight ellipsoidal inclusions, $a = 0.05, b = 0.05, c = 0.15$, volume fraction $\rho = 0.01257$

As we have several inclusions in this case, the reference solution is given by the analytical Self-Consistent Model (SCM) [9], based on the Eschelby's tensor [4].

We also notice a linear convergence for both thermal and elastic cases, see Figure 17. This observation proves that FDMH responds properly to the cases with numbers of inclusions.

4.5. Pellicle / Hollow sphere inclusion

We consider a pellicle sphere inclusion, centered with $d = 0.6$, as shown in Figure 18. The reference solution is given by a three phases Mori-Tanaka model based on the Eshelby inclusions [13]. Numerical tests are performed with different relative

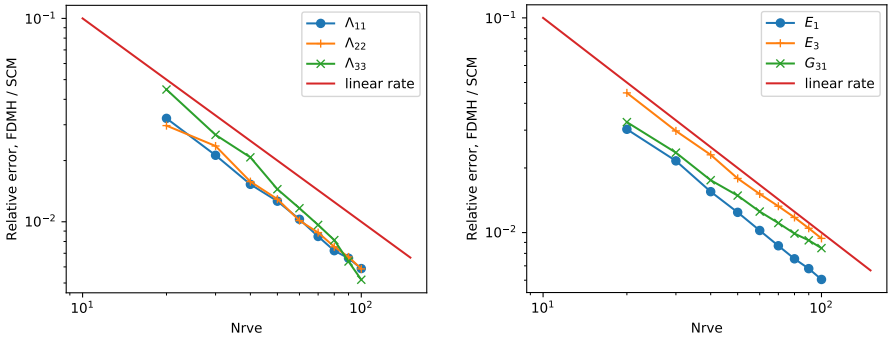

Figure 17: Relative error of the homogenized conductivity tensor (left) and stiffness coefficients (right) for eight ellipsoidal inclusions case

thickness, which is defined as the ratio between the thickness of the pellicle and the radius of the sphere.

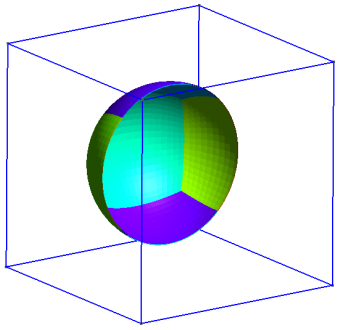

Figure 18: RVE with one pellicle spherical inclusion with $d = 0.6$, relative thickness = 0.01

In Figure 19, the homogenized coefficients λ are normalized and plotted versus the relative thickness for both FDMH and Mori-Tanaka solution. The results computed by these two methods are close. With a relative thickness equal to 0.01, the relative difference is about 1%. We conclude that the FDMH can be used to compute effective properties of periodic material with very thin pellicle inclusions. We also note that for the inclusions computation, a 2 dimensional model can be used. This ability to consider very thin inclusions is an interesting advantage of the FDMH over other numerical homogenization methods.

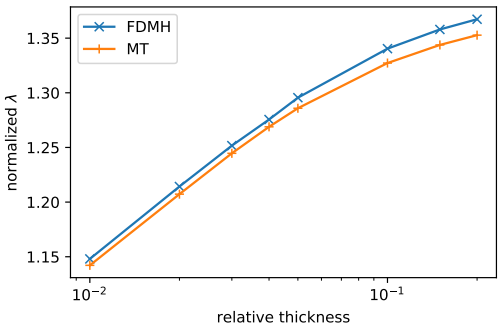

Figure 19: Relative error of computed homogenized conductivity coefficient λ against the relative thickness for one pellicle sphere inclusion

Computing resources

The computations are performed by a finite element library code, named CFEM, developed by the authors, in Python/Fortran. We use the PETSc[1] library to solve the linear systems. The meshes are generated with the Gmsh software [6].

In some cases, as the RVE resolution may involves millions of DOFs, we used Myria, a HPC cluster located in CRIANN[2]. However, all of the computations presented in this paper can be performed on personal computers (We used a 2014 macbook pro laptop or a laptop PC).

5. Conclusion

We have presented an original alternative method to evaluate the effective properties of periodic heterogeneous materials, using a fictitious domain principle. With the help of a connection matrix between the distinct meshes of inclusions and RVE, we are able to implement a finite element in the framework of a structured mesh of the RVE.

Numerical tests, with inclusions of elementary geometry such as sphere, cube and ellipsoid, have shown a linear convergence of relative errors with respect to reference solutions. The convergence rates are observed as expected, regarding the use of linear interpolation.

One interesting advantage of the FDMH method presented in this paper is the total flexibility concerning the inclusions meshes. Complex geometries of any kind can be considered, as long as a mesh is available. We have shown an example with very thin spherical pellicle, but we can also imagine a case of a very high resolution 3d image of a composite material sample, obtained through imagery techniques, such as tomography. We can obtain the (fine) meshes of the inclusions by segmentation techniques and then consider a coarser mesh of the sample, making the computation possible.

[1]Portable, Extensible Toolkit for Scientific Computation : https://www.mcs.anl.gov/petsc
[2]Regional Computer Center and Digital Applications of Normandy : https://www.criann.fr

With the cubic inclusion test where we have been able to give an estimation the error of the FDMH compared to a classical finite element method with a mesh conforming to the inclusions geometry. These substantial errors indicates that improvement of the efficiency of the method should be developed. In particular, we are currently investigating how to introduce some kind of enrichment by modifying the connection matrix in order to better conform the weak continuity at interfaces.

[1] Bechterew, P. *Analytical study of the generalized hooke's law, application of the method of coordinate transformation.* Zh Russ Fiz-khim Obshch Leningrad Univ Fizika 58, 3, 1926, 415-446

[2] Benveniste, Y. *A new approach to the application of Mori-Tanaka's theory in composite materials.* Mechanics of Materials 6, 1987, 147-157

[3] Buryachenko Valeriy A. *Micromechanics of Heterogeneous Materials* Springer, 2007

[4] Eshelby, J.D. *The determination of the elastic field of an ellipsoidal inclusion and related problems.* Proceedings of the Royal, Society London A241, 376.

[5] Debordes, O. *Homogenization Computations in the Elastic or Plastic Range. Applications to Unidirectional Composite and Perforated Sheets Computational Mechanics.* Proceedings of the 4th International Symposium Innovative Numerical Methods in Engineering, 1986, 453-458

[6] Geuzaine, C. and Remacle, J.-F. *Gmsh: a three-dimensional finite element mesh generator with built-in pre- and post-processing facilities.* International Journal for Numerical Methods in Engineering, 2009, 79(11), 1309-1331

[7] R. Glowinski, T. Pan and J. Periaux *A fictitious domain method for Dirichlet problem and applications.* Computational Methods Applied to Mechanical Engineering., 1994, 111, 283-303

[8] Hatta, H. and Taya, M. *Equivalent inclusion method for steady state heat conduction in composites.* International Journal of Engineering Science, 1986, 24, 1159-1170

[9] Hill, R. *A self-consistent mechanics of composite materials.* Journal of the Mechanics and Physics of Solids 13, 4, 1965, 213-222

[10] G.Legrain, M. Chevreuil and N. Takano *Prediction of apparent properties with uncertain material parameters using high-order fictitious domain methods and PGD model reduction.* International Journal for Numerical Methods in Engineering, Wiley, 2016

[11] Alexander Düster, Hans-Georg Sehlhorst, Ernst Rank *Numerical homogenization of heterogeneous and cellular materials utilizing the Finite Cell Method.* Computational Mechanics (2012) 50: 413

[12] Nikolai S. Bakhvalov, Andrew V. Knyazev. *Fictitious domain methods and computation of homogenized properties of composites with a periodic structure of essentially different components.* Numerical Methods and Applications (1994). CRC Press.

[13] Le Quang, H., Bonnet, G., and He, Q.-C. *Size-dependent Eshelby tensor fields and effective conductivity of composites made of anisotropic phases with highly conducting imperfect interfaces.* Physical Review B : Condensed matter and materials physics 81, 6 (2010), –.

[14] Bensoussan, A.; Lions, J.-L. and Papanicolaou, G. *Asymptotic analysis for periodic structures.* North-Holland Publishing Company Amsterdam, 1978, 5

[15] Moës, N. , Dolbow, J. and Belytschko, T, *A finite element method for crack growth without remeshing.* International Journal for Numerical Methods in Engineering, 1999, 46:131-150

[16] Moulinec, H. and Suquet, P. *A fast numerical method for computing the linear and nonlinear mechanical properties of composites.* Comptes rendus de l'Académie des sciences. Série II, Mécanique, physique, chimie, astronomie, Elsevier, 1994, 318, 1417-1423

[17] Moulinec, H. and Suquet, P. *A FFT based-numerical method for computing the mechanical properties of composites from images of their microstucture.* No.1 R.Pyrz, Ed., Microstructure-Property Interactions in Composites Materials, 1995

[18] Mori, T. and Tanaka, K. *Average stress in matrix and average elastic energy of materials with misfitting inclusions.* Acta Metallurgica 21, 5, 276-283, 1973

[19] Tosio Mura. *Micromecanics of Defects in Solids.* Martinus Nijhoff Publishers, 1980

[20] Sanchez-Palencia, E. and Sanchez-Hubert, J. *Introduction aux méthodes asymptotiques et à l'homogénéisation - Application à la mécanique des milieux continus.* Masson, 1992

[21] Schneider, K.; Klusemann, B. and Bargmann, S. *Automatic three-dimensional geometry and mesh generation of periodic representative volume elements for matrix-inclusion composites.* Advances in Engineering Software, Elsevier, 2016, 99, 177-188

[22] Stransky, J.; Vorel, J.; Zeman, J and Sejnoha, M. *Mori-Tanaka based estimates of effective thermal conductivity of various engineering materials.* Micromachines 2011, 2, 129-149

[23] Sukumar, N. Chopp, D. L. Moës, N. and Belytschko, T, *Modeling holes and inclusions by level sets in the extended finite-element method.* Computer methods in applied mechanics and engineering, Elsevier, 2001, 190, 6183-620

[24] Julien Yvonnet, H. Le Quang, Qi-Chang He. *An XFEM/level set approach to modelling surface/interface effects and to computing the size-dependent effective properties of nanocomposites.* Computational Mechanics, Springer Verlag, 2008, 42(1), 704-712